Published by IOP Publishing for Sissa Medialab

Received: *November 7, 2023*
Revised: *December 10, 2023*
Accepted: *December 21, 2023*
Published: *January 2, 2024*

Research on multi-probe energy response compensation for X/γ dose rate meter

M. Li,[a] P. Gong,[a,b,*] H. Zhang,[c] Zh. Hu,[a,b] P. Wang,[c] Z. Wang,[a] D. Liang,[a] Ch. Zhou,[e] X. Zhu,[e] G. Gorini,[f] G. Croci[f] and X. Tang[a,b]

[a] *Department of Nuclear Science and Technology, Nanjing University of Aeronautics and Astronautics, Nanjing 210016, China*
[b] *Key Laboratory of Nuclear Technology Application and Radiation Protection in Astronautics, Ministry of Industry and Information Technology, Nanjing 210016, China*
[c] *National Institute of Metrology, Beijing 100029, China*
[d] *School of Environmental and Biological Engineering, Nanjing University of Science and Technology, Nanjing 210094, China*
[e] *Jiangsu Nuclear and Radiation Safety Supervision and Management Center, Nanjing 210019, China*
[f] *Department of Physics, University of Milan-Bicocca, Milan 20126, Italy*

E-mail: gongpin@nuaa.edu.cn

Abstract: Dose rate meters operating in pulse counting mode usually encounter the problem of uneven energy response. While current methods of coating a single probe with a metal layer can effectively improve the flatness of the energy response, the energy range of the flat response is limited. In this research, a multi-probe energy response compensation method was proposed to solve the problem of uneven energy response of a CsI(Tl) dose rate meter. In this method, different relative energy response curves were obtained by adding different hardware compensations to a probe. Then, two to four relative energy response curves were selected and weighted to obtain a flatter response within the energy region of interest. Specifically, first, 51 compensation schemes were obtained by changing the geometry and material parameters of the CsI(Tl) probe compensation layer. Second, the relative energy response curves of CsI(Tl) probes with 51 compensation schemes were obtained by MCNP simulation. Finally, the weight coefficient of each relative energy response curve was determined by overdetermined equations, and the combination with the smallest relative energy response deviation was selected. Within the energy range of 80–1500 keV, the optimal two-probe compensation scheme was selected from one to three probe compensation schemes. After the dual

*Corresponding author.

https://doi.org/10.1088/1748-0221/19/01/P01005

probe combination compensation, the relative energy response deviation ranged from −23.0% to 5.0%. Within the energy range of 50–3000 keV, the compensation schemes of one to four probes were traversed. The optimal three-probe compensation schemes were selected. After combined compensation, the relative energy response deviation ranged from −27.3% to 15.3%. Furthermore, the compensation effect of multiple probes was better than that of single probes in both energy regions of interest. Simulation results demonstrated that our proposed method can significantly improve the flatness of the energy response of dose rate meters based on CsI(Tl).

KEYWORDS: Models and simulations; Solid state detectors; Detector design and construction technologies and materials; Detector modelling and simulations I (interaction of radiation with matter, interaction of photons with matter, interaction of hadrons with matter, etc)

2024 JINST 19 P01005

Contents

1 Introduction

Dose rate meters play an important role in ensuring radiation safety, identifying emergency situations, and avoiding serious radiation accidents. Some dose rate meters are used for radiation protection monitoring, measuring $H^*(10)$ [1–3], while others are used for environmental dose rate monitoring, measuring air-absorbed dose rate [4–6]. Currently, most dose rate meters primarily operate in pulse counting mode. In this mode, when the meters measure the absorbed dose rate in the air, their primary concern is the quantity of pulses detected, and they do not consider the pulse amplitude (i.e., the energies of incident photons). Therefore, the uneven energy response of the dose rate meters will result in different pulse counts if the energy of γ photons is different at the same air-absorbed dose rate. To accurately measure the air-absorbed dose rate of X/γ rays of different energies, the detector must thus respond consistently to X/γ rays of different energies. However, scintillating crystal-based dose rate meters such as NaI(Tl) and CsI(Tl) respond unevenly to X/γ rays of different energies [1, 7–12]. For example, in Park's research, the uncompensated CsI(Tl) dose rate meter had a relative energy response of 33 (relative to ^{137}Cs) at 100 keV and 0.45 at 1250 keV [8]. Obviously, the energy response of the uncompensated CsI(Tl) dose rate meter varied greatly.

Hardware compensation is a prevalent approach to solve the non-uniformity of energy response [8–12]. This method involves enveloping the probe with a thin metal enclosure to screen out a fraction of low-energy photons from interacting with the detector crystal, effectively curtailing the relative energy response of the detector within the low-energy range (50–300 keV). It is also customary to make holes in the compensation layer in order to prevent excessive attenuation of low-energy X/γ rays. The compensatory efficacy of the hardware compensation approach has been validated through many research efforts [13–17].

Although the energy response flatness of the dose rate meter with hardware compensation has been obviously improved compared with that before compensation, the problem remains that the response flatness area is too narrow [15–17]. It could not satisfy the Chinese Standard HJ 1157-2021 [18], which stated that the relative response deviation should be between -30% and 30% in the energy range

2024 JINST 19 P01005

of 50–3000 keV. The use of multiple probes to optimize the response of the detector has been studied in the field of long neutron counter, and good results have been obtained, which provided an idea for solving the problem of uneven response of X/γ dose rate meters [19–21].

Consequently, to further optimize the energy response flatness of scintillation crystal detectors, the present study introduced a multi-probe energy response compensation method. The proposed method was subsequently validated using MCNP simulations.

2 Method and principle

Figure 1 shows the principle of the multi-probe energy response compensation method. First, 51 compensation schemes were obtained by changing the material and size of the compensation layer of the probes. The 51 energy response curves corresponding to the 51 compensation schemes were obtained using MCNP simulations. Next, a target number of probes were selected and appropriate weighting factors for these probes were calculated. Finally, the relative energy response curves of the selected probes were weighted and combined to obtain relative energy response curves that are relatively flat over a wide energy region.

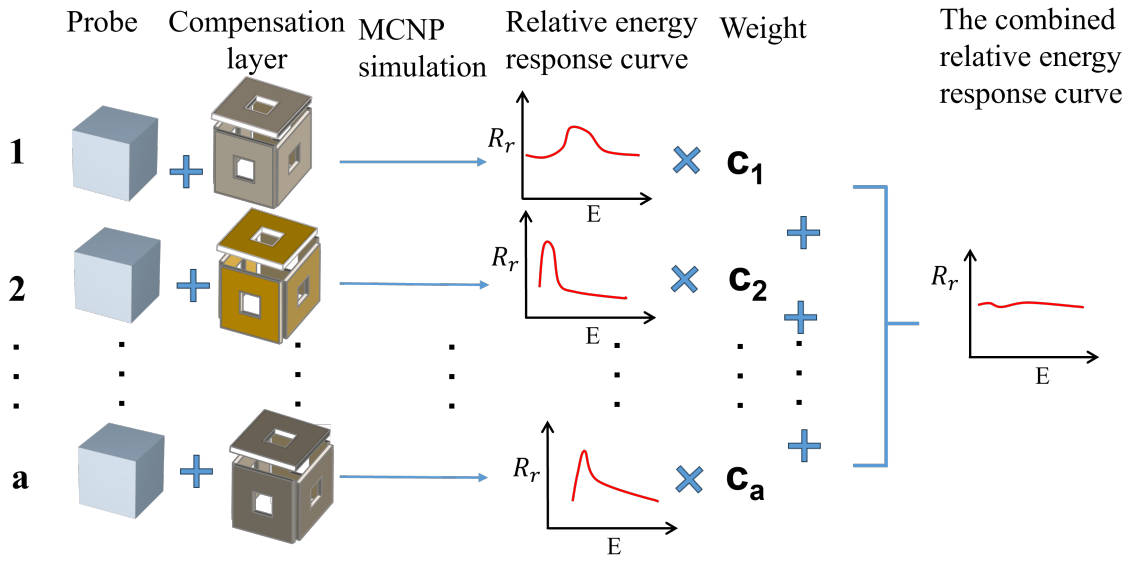

Figure 1. Principle of multi-probe energy response compensation.

2.1 Relative energy response calculation

This section focuses on the calculation of the relative energy response determined by MCNP.

When the energy of the X/γ ray incident into the detection medium was E_i, the energy response of the detector was calculated by equation (2.1):

$$r(E_i) = \frac{n(E_i)}{\dot{D}_T(E_i)}, \tag{2.1}$$

where r is the energy response; n is the count rate measured by the dose rate meter, in the unit s^{-1}; $\dot{D}_T$ is the true value of the absorbed dose rate of the air, in the unit Gy/s; and E_i is the energy of incident X/ γ rays.

2024 JINST 19 P01005

Generally, the relative energy response (relative to ^{137}Cs) is used to evaluate the energy response characteristics. Therefore, the energy response should be normalized using the response value of the dose rate instrument at 662 keV to obtain the relative energy response R_r:

$$R_r(E_i) = \frac{r(E_i)}{r(662\,\text{keV})}. \tag{2.2}$$

2.2 MCNP simulation

A model of CsI(Tl) crystals with dimensions of 25 mm × 25 mm × 25 mm was constructed in MCNP. The top and sides of the crystal were covered with a 0.5 mm-thick magnesium oxide reflector and compensation layer. The bottom of the crystal was reserved for signal output, without any covering reflector and compensation layer. Furthermore, square apertures were introduced at the center of each compensation layer (figure 2).

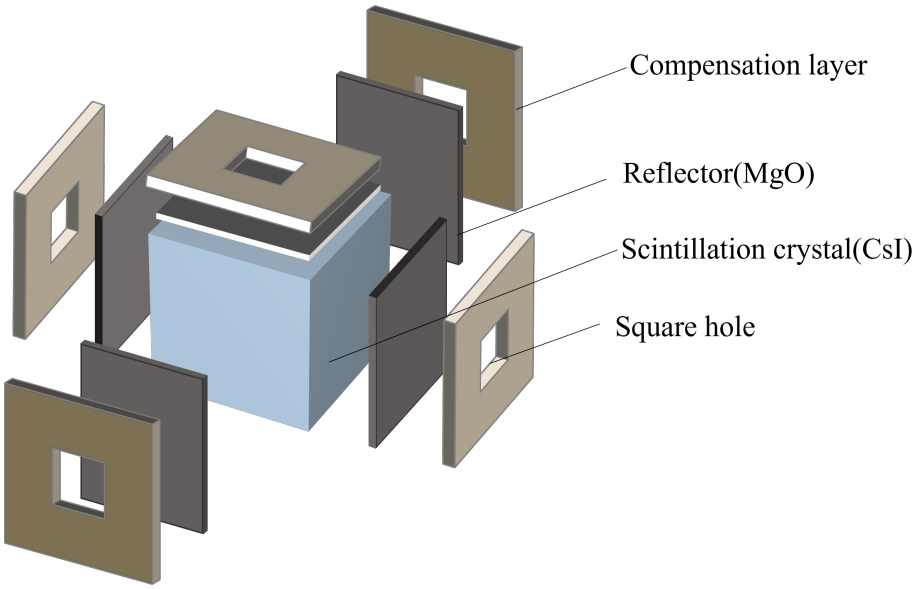

Figure 2. Schematic diagram of the probe crystal compensation structure.

During the simulation process, the shielding effectiveness and cost-effectiveness of compensation materials were taken into consideration. Four types of metals, namely, Pb, Sn, Cu, and Al, were chosen. The relative energy response curves of 51 kinds of single-probe compensation were simulated, including 16 compensation schemes for 4 kinds of metals of 1–4 mm thickness without holes. There are also 25 compensation schemes using Pb, with the thickness of the Pb compensation layer ranging from 1 to 10 mm and the length of the holes being 6, 8, and 10 mm, and 10 compensation schemes using Sn, with the thickness of the tin compensation layer ranging from 2 to 6 mm and the length of the holes being 6 mm and 8 mm.

The radiation source was configured as a point source and positioned at a distance of 3 m from the detector. X/γ photons were incident from the upper surface of the crystal. In each simulation run, a total of 50 million source particles were employed, thus maintaining statistical robustness. The calculation of the energy response is described in section 2.1, and the MCNP simulation acquires the two variables in equation (2.1). The count rate n was obtained by counting the total number of pulses in the

2024 JINST 19 P01005

CsI crystal using pulse height tally (tally type 8). The air-absorbed dose rate truth value $\dot{D}_T$ is obtained using energy deposition tally (tally type 6) after replacing the CsI crystal with an equal volume of air.

The radiation sources in the simulation were divided into three types: measured X-ray source, reference X-ray source, and single energy source. Considering the actual experimental conditions, the X-ray energy spectra of the MG325 X-ray machine with corresponding filter were obtained by Trans-SPEC-N HPGE detector in Jiangsu Institute of Metrology. The X-rays were generated according to the guidelines set out in the ISO 4037-1:2021 standard [22]. The measured N-series spectra and their corresponding average energies presented in the "Source 1" section of table 1. Given the limited achievable energy points of the X-ray tube, the reference spectra from the ISO 4037-1:2021 standard were incorporated to supplement the entries under "Source 2" in the table 1. For the high-energy range, single-energy point sources were utilized. A total of 33 energy points were evenly spaced from 330 keV to 660 keV, while an additional 23 energy points were evenly distributed between 700 and 3000 keV. A ^{137}Cs source with an energy of 662 keV was introduced to simulate data for normalization purposes.

Table 1. X-ray source.

Radiation quality	Average Energy (keV)	Source	Radiation quality	Average Energy (keV)	Source
N-60	48	1	N-200	165	1
N-80	65	1	N-250	207	1
N-100	83	1	N-300	248	2
N-120	100	1	N-350	288	2
N-150	118	1	N-400	328	2

2.3 Compensation combination selection and coefficient determination

This section introduces a methodology to ascertain the optimal combination compensation plan and the corresponding weight coefficients for each probe during the compensation process.

After 51 relative energy response curves were obtained from the simulation, a further step was to determine which probes (curves) were to be combined and the weighting factors for each probe. Selecting k ($k > 1$) probes (curves) from n probes (curves) for combination was a random process, and the total number of combinations was N, $N = C_n^k$, where k is the number of target probes used to combine compensation, and n is the total number of probes available for selection. For example, 2 probes were selected from 51 probe compensations resulting in $C_{51}^2 = 1275$ combinations. Furthermore, for each of the N combinations, appropriate weight coefficients were assigned to each probe. The relative energy response curves of all combinations were then calculated, and the combination with the smallest energy response deviation was selected as the final compensation scheme.

The determination of weight coefficient was a process of solving overdetermined equations using equation (2.3):

$$R_{\text{target}} = \sum_k R_i \cdot c_i, \tag{2.3}$$

where R_{target} is a $j \times 1$ target relative energy response matrix, with j being the number of energy points selected within the energy response range. The ideal energy response result is for the relative

2024 JINST 19 P01005

energy response of each energy point to be 1 so that all elements in the matrix are 1. R_i is a $j \times 1$ relative energy response matrix, specifying the response of the ith probe out of the a probes selected. c_i is the weight coefficient of the ith probe.

We then have equation (2.4):

$$R_{\text{target}} = R \cdot c, \tag{2.4}$$

For the overdetermined system of equations determined by equation (2.4), we aim to minimize the residual Δ between the target response and the combined response, as expressed in equation (2.5).

$$\Delta = \| R_{\text{target}} - Rc \|_2 = \min \| R_{\text{target}} - Rc \|_2 . \tag{2.5}$$

Then, we can obtain the least squares solution of the system, which is the vector coefficient c:

$$c = (R^T R)^{-1} R^T R_{\text{target}}. \tag{2.6}$$

3 Results and discussion

The International Electrotechnical Commission and the Ministry of Ecology and Environment of the People's Republic of China have different requirements for the energy response of dose rate meters. The international standard IEC61017-2012 [23] requires that the relative energy response deviation be from −30% to 30% in the energy range of 80–1500 keV. The energy response requirement according to the Chinese standard HJ1157-2021 specifies that within the energy range of 50–3000 keV, the deviation in relative energy response should remain within the range of −30% to 30%. The compensation results will be discussed separately in terms of the energy intervals specified in these two standards.

3.1 Single-probe compensation results

The uncompensated relative energy response of the CsI(Tl) dose rate meter is shown as the black line in figure 3(a). Clearly, without compensation, the relative energy response of the CsI(Tl) dose rate meter in the low-energy region (30–300 keV) has a large value, with a response value of 9 or more near 70 keV energy. By contrast, the relative energy response in the high-energy region (2000–3000 keV) is low, only about 0.3 at 3000 keV. In the absence of shielding compensation, CsI(TI) dose rate meters exhibit significant differences in relative energy response and, therefore, require compensation.

The compensation capacity of the four selected metals is positively correlated with their atomic number. As shown in figure 3(a), when the thickness of the shielding layer is the same, the compensation capacity for the low-energy region (30–300 keV) is Pb>Sn>Cu>Al. It can likewise be observed that the relative energy response of the CsI(Tl) probe remains relatively stable in the high-energy region, with limited compensation effect from the non-porous metal layer. Therefore, it is necessary to try to make holes in the compensation layer.

The situation of opening square holes on compensation layers of different thicknesses was simulated. Among them, the results of opening square holes of 6 mm side length on Pb compensation layers of different thicknesses are shown in figure 3(b). The relative energy response of the open aperture to 30–200 keV was found to be significantly enhanced when the Pb compensation was used. Moreover, with the increase of Pb thickness, the relative energy response of the CsI(Tl) probe increased at 30–250 keV and 660–3000 keV but decreased at 300–660 keV.

2024 JINST 19 P01005

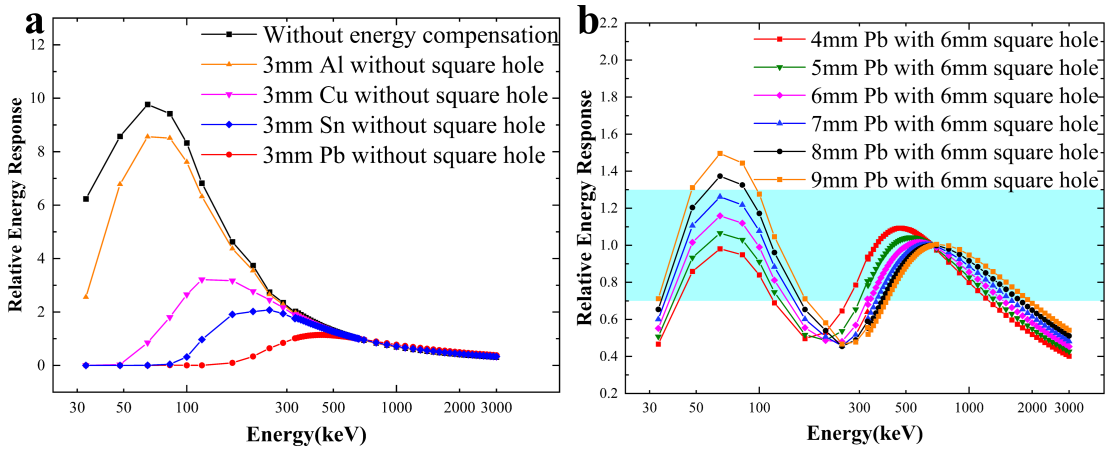

Figure 3. (a) Compensation result without hole for the 3 mm compensation layer. (b) Compensation result for the 6–10 mm-thick Pb compensation layer with 6 mm hole edge length.

For the two standards, the results with the smallest relative standard deviation were selected from the 51 single-probe compensated relative energy response curves shown in figure 4. Figure 4(a) shows the results of the single-probe optimal compensation in the energy range of 80–1500 keV as specified in IEC60107-2012. The compensating material is a 5 mm-thick lead layer with a 6 mm edge length square hole in the center of the layer. In the energy ranges 150–250 keV and 1350–1500 keV, the deviation of the relative energy response is clearly more than -30%, thus failing to meet the required standard. Considering the energy range of 50–3000 keV specified by HJ1157-2021, the single-probe compensation scheme with 7 mm-thick Pb and 6 mm square hole edge length has the minimum standard deviation. The relative energy response after compensation is shown in figure 4(b). Although the compensated relative energy response of this scheme shows a significant improvement over the pre-compensation response, the deviation of the relative energy response is less than -30% in the energy region from 150 keV to 350 keV and above 1500 keV. Therefore, the results of single-probe compensation cannot meet the requirements of HJ1157-2021.

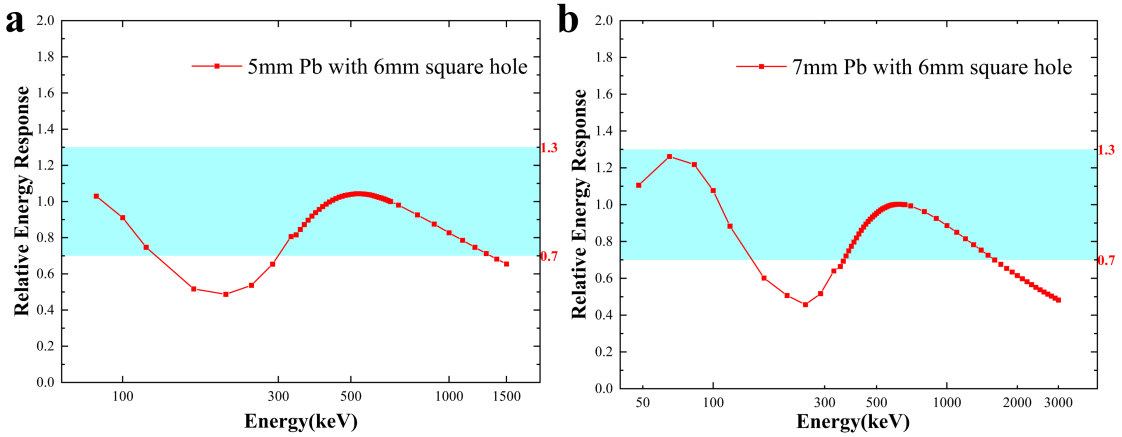

Figure 4. (a) Single-probe optimal compensation curve: 80–1500 keV single-probe optimal compensation relative energy response curve. (b) 50–3000 keV single probe optimal compensation relative energy response curve.

2024 JINST 19 P01005

3.2 Multi-probe compensation results

For the energy region from 80 keV to 1500 keV specified in the IEC61017-2012 standard, the optimal two-probe combination compensation results are shown in figure 5(a). The combination of the compensation scheme of 4 mm-thick Sn without holes (blue line) and the compensation scheme of 10 mm-thick Pb with square holes (green line) with a side length of 6 mm is chosen. Furthermore, the relative energy response deviation ranges from −23.0% to 5.0% within the energy range of 80–1500 keV after the combination (red line), which meets the requirements of the relative energy response deviation of IEC61017-2012. The optimal compensation scheme when the number of probes is increased to three is shown in figure 5(b). The compensation schemes for the three probes are the 1.5 mm-thick Pb compensation layer without holes (blue line), 5 mm-thick Pb compensation layer with square holes with 8 mm sides (green line), and 6 mm-thick Pb compensation layer with square holes with 8 mm sides (black line). The relative energy response deviation is −24.8% to 23.5% in the 80–1500 keV energy region after the three-probe combination (red line). Figure 5(c) shows the results after compensation with different numbers of probes. It can be found that the relative energy response curve of the two-probe and three-probe combinations after compensation does not differ much in the 300–1500 keV energy region. Overall, the relative energy response curve after compensation of

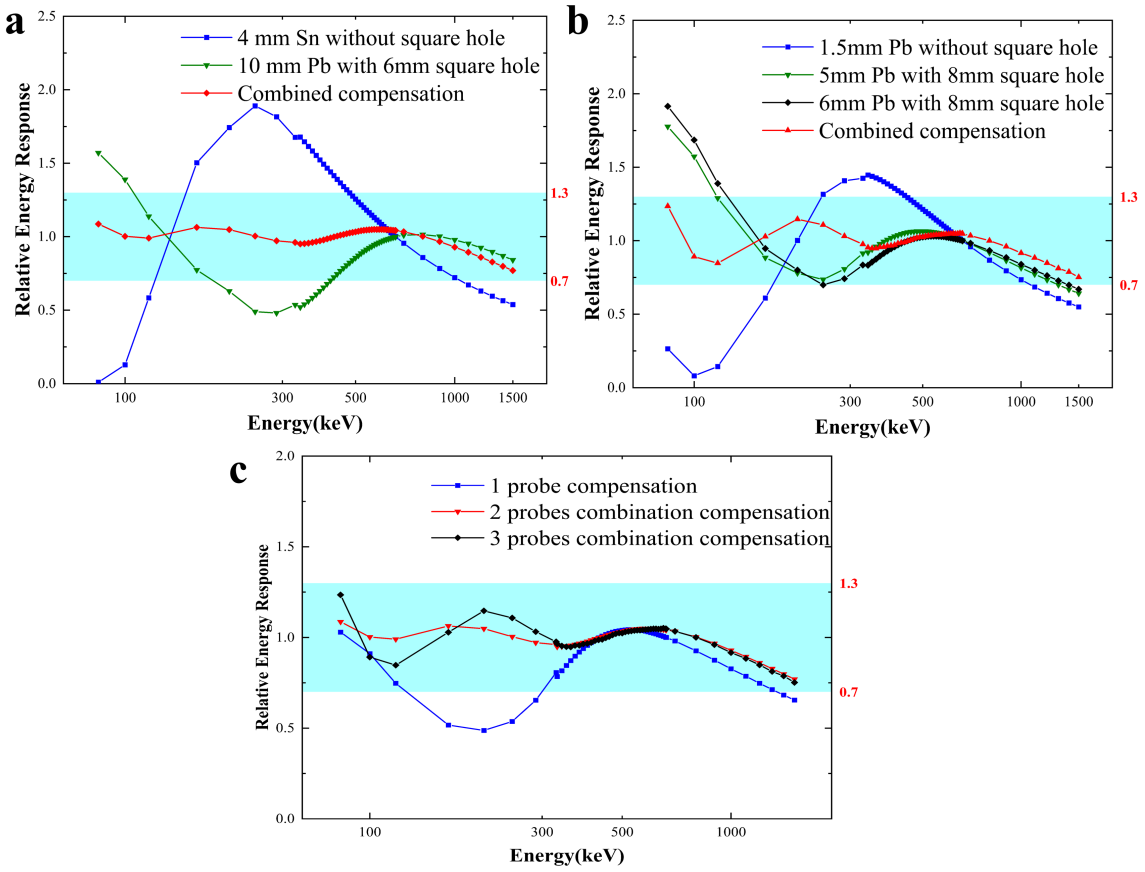

Figure 5. 80–1500 keV compensation results: (a) dual probe, (b) three probes, (c) comparison of the 1–3 probe compensation results.

2024 JINST 19 P01005

the two-probe combination is flatter than that of the three-probe. In addition, the relative standard deviation of the compensated relative energy response curve is 0.0843 for the three probes and 0.0670 for the two probes. Therefore, in the energy range of 80–1500 keV, the relative energy response deviation of the three-probe and two-probe compensations meet the standard IEC61017-2012, and after comparison, the two-probe compensation scheme is recommended.

The energy response requirement according to the Chinese standard HJ1157-2021 specifies that within the energy range of 50–3000 keV, the deviation in relative energy response should remain within the range of −30% to +30%. The results of multi-probe compensation are shown in figure 6. The compensation results after the number of probes is increased to 2 are shown in the red line in figure 6(a). The deviation of relative energy response after combined compensation is greater than 30% in the energy region above 2100 keV. The compensation result when the number of probes is 3 is shown in figure 6(b). Within 50–3000 keV, the relative energy response deviation is within −27.3% to 15.3%. The compensation results when the number of probes is 4 are shown in figure 6(c). The deviation of relative energy response in the 50–3000 keV energy region is −25.3% to 17.0%. The three-probe and four-probe combinations meet the standard HJ1157-2021 after compensation. Note that when multiple probes are used to compensate, the thickness of the lead compensation layer used in the combination reaches 8–10 mm, which will significantly increase the weight of the detector. Additionally, the detector after compensation by this scheme will be more suitable for fixed monitoring equipment. A comparison of the compensation results for different numbers of probes, as shown in figure 6(d), reveals that the compensation effect improves as the number of probes increases. The relative energy response curves of the three probes and four probes after compensation have little difference in the energy range above 300 keV. The obvious difference is that the relative energy response value of the four probes after compensation is closer to 1 at the range of 65–300 keV, which is better than that of the three probes. As the number of probes increases from three to four, there is a slight improvement in the flatness of the combined relative energy response curve. Hence, a three-probe compensation scheme is recommended.

4 Conclusions

In this study, a multi-probe energy response compensation method was proposed, wherein distinct hardware compensation and weighting coefficients were applied to multiple CsI(Tl) probes. The combined compensation achieved a flat energy response in the energy range of interest. The relative energy response curves of 51 compensation schemes were obtained by MCNP simulation, and the best combined compensation schemes were determined in the energy range of 80–1500 keV and 50–3000 keV. The optimal compensation scheme of double probe was determined in the energy range of 80–1500 keV. After the combination compensation, the relative energy response deviation was between −23.0% and 5.0%, which met the requirement of IEC61017-2012. In addition, the relative energy response deviation of the three-probe combination after compensation was −27.3% to 15.3% in the energy range of 50–3000 keV, which met the standard HJ1157-2021. The compensation effect of multiple probes was also better than that of single probes in both energy regions of interest. Therefore, this study demonstrated with simulations that the multi-probe energy response compensation method has a significant optimization effect on the relative energy response of the detector.

In future studies, attempts will be made to apply this method to other types of dose rate meters, such as GM counting tube-based dose rate meters and CZT based dose rate meters.

2024 JINST 19 P01005

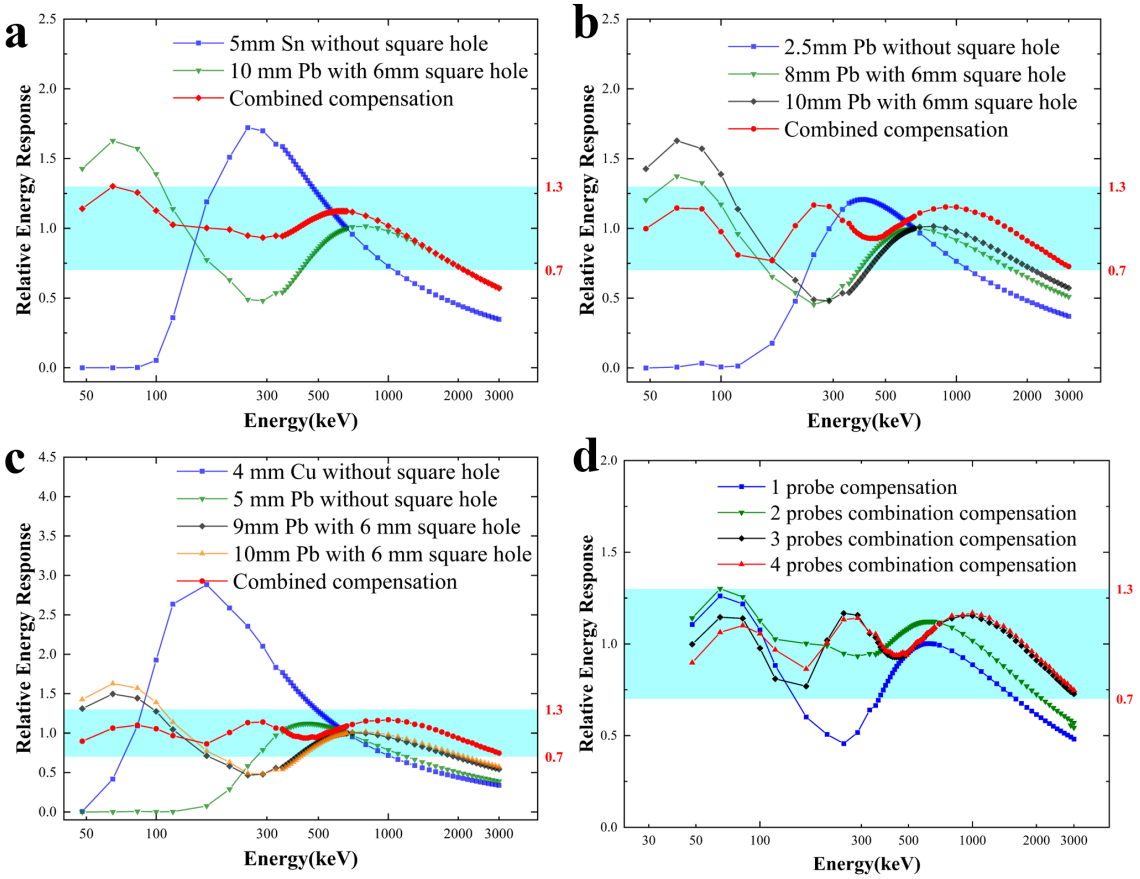

Figure 6. 50–3000 keV compensation results: (a) dual probes, (b) three probes, (c) four probes, (d) comparison of the 1–4 probe compensation results.

Acknowledgments

This work was supported by National Natural Science Foundation of China (No. 12105144), the Primary Research and Development Plan of Jiangsu Province (Grant No. BE2022846, BE2023816), China Postdoctoral Science Foundation (Grant No. 2022M721659), and the Fundamental Research Funds for the Central Universities (Grant No. NC2022006, NG2023002).

References

[1] K. Park et al., *Improvement of a spectrum-to-dose conversion function for electronic personal dosimeters*, 2020 *JINST* **15** C02018.

[2] P. Buzhan, A. Karakash and Y. Teverovskiy, *Silicon Photomultiplier and CsI(Tl) scintillator in application to portable $H^*(10)$ dosimeter*, *Nucl. Instrum. Meth. A* **912** (2018) 245.

[3] S. Tsuda et al., *Analyses of $H^*(10)$ dose rates measured in environment contaminated by radioactive caesium: correction of directional dependence of scintillation detectors*, *Radiat. Prot. Dosimetry* **193** (2021) 228.

[4] S. Tsuda and K. Saito, *Spectrum-dose conversion operator of NaI(Tl) and CsI(Tl) scintillation detectors for air dose rate measurement in contaminated environments*, *J. Environ. Radioact.* **166** (2017) 419.

2024 JINST 19 P01005

[5] P. Mitra et al., *Countrywide monitoring of absorbed dose rate in air due to outdoor natural gamma radiation in India*, *Radiat. Prot. Dosimetry* **199** (2023) 1336.

[6] Y. Shiroma et al., *Changes of absorbed dose rate in air by car-borne survey in Namie town, Fukushima prefecture after the Fukushima Daiichi nuclear power plant accident*, *Radiat. Prot. Dosimetry* **184** (2019) 527.

[7] J. Hwang et al., *Estimation of ambient dose equivalent rate with a plastic scintillation detector using the least-square and first-order methods-based G(E) function*, *Appl. Radiat. Isot.* **194** (2023) 110707.

[8] K. Park et al., *Ambient dose equivalent measurement with a CsI(Tl) based electronic personal dosimeter*, *Nucl. Eng. Technol.* **51** (2019) 1991.

[9] Z. Li et al., *Optimization for energy response characteristics of plastic scintillators based on genetic algorithm*, *AIP Adv.* **12** (2022) 115111.

[10] S.M. Taheri Balanoji, H. Zaki Dizaji and A. Abdi Saray, *Photon dosimetry using selective data sampling with Particle Swarm optimization algorithm based on NaI(Tl) scintillation detector*, *Kerntechnik* **87** (2022) 364.

[11] P. Kessler, B. Behnke, H. Dombrowski and S. Neumaier, *Characterization of detector-systems based on CeBr 3 , LaBr 3 , SrI 2 and CdZnTe for the use as dosemeters*, *Radiat. Phys. Chem.* **140** (2017) 309.

[12] Y.D. Wu et al., *Comparison of two spectrum-dose conversion methods based on NaI(Tl) scintillation detectors*, 2018 *JINST* **13** T06004.

[13] P. Wang et al., *Design of a portable dose rate detector based on a double Geiger-Mueller counter*, *Nucl. Instrum. Meth. A* **879** (2018) 147.

[14] N. Kržanović et al., *Development and testing of a low cost radiation protection instrument based on an energy compensated Geiger-Müller tube*, *Radiat. Phys. Chem.* **164** (2019) 108358.

[15] R.B. Wang and K. Yang, *MC Simulation of sodium iodide detector energy response and its optimal design*, *Nucl. Electron. Detect. Technol.* **35** (2015) 188.

[16] X.M. Zhou, G.M. Liu and Y.Z. Chen, *Optimization design for energy response of the mobile radioactive gas monitor*, *Nucl. Tech.* **41** (2018) 030401.

[17] J.H. Zhong, L.Q. Ge, J. Zhang, Q.X. Zhang and J. Yang, *Energy Response Compensation of MCNP Simulated Lanthanum Bromide Detector*, *Sci. Technol. Eng.* **20** (2020) 8590

[18] HJ1157-2021, https://www.mee.gov.cn/ywgz/fgbz/bz/bzwb/jcffbz/202104/t20210429_831308.shtml.

[19] H. Harano et al., *Development of a Compact Flat Response Neutron Detector*, *IEEE Trans. Nucl. Sci.* **58** (2011) 2421.

[20] P. Wang et al., *Design of a compact long counter with an improved response using multiple point-like thermal neutron counters*, *Eur. Phys. J. Plus.* **138** (2023) 419.

[21] K. Watanabe et al., *Flat-response neutron detector using spatial distribution of thermal neutrons in a moderator*, *Nucl. Instrum. Meth. A* **652** (2011) 392.

[22] International Organization for Standardization, *Radiological protection — X and gamma reference radiation for calibrating dosemeters and doserate meters and for determining their response as a function of photon energy — -part 3: calibration of area and personal dosemeters and the measurement of their response as a function of energy and angle of incidence*, ISO 4037-3:2019.

[23] International Electrotechnical Commission, *Radiation protection instrumentation — Transportable, mobile or installed equipment to measure photon radiation for environmental monitoring*, IEC 61017-2016.

2024 JINST 19 P01005